

Evaluating damage extent of fractured beams in steel moment-resisting frames using dynamic strain responses

Xiaohua Li¹, Masahiro Kurata², and Masayoshi Nakashima²

¹*Department of Architecture and Architectural Engineering, Kyoto University, Kyoto, Japan*

²*Disaster Prevention Research Institute, Kyoto University, Kyoto, Japan*

SUMMARY

Delays in the post-earthquake safety estimations of important buildings significantly increase unnecessary disorder in economic and social recovery following devastating earthquakes. Providing promptness and objectivity in evaluation procedures, damage detection through a structural health monitoring system using sensors attracts attention from building owners and other stakeholders. Nonetheless, local damage on individual structural elements is not easily identifiable, as such damage weakly relates to the global vibrational characteristics of buildings. The primary objectives of this research are to present and verify a method that quantifies the amount of local damage (i.e., fractures near beam-column connections) for the health monitoring of steel moment-resisting frames that have undergone a strong earthquake ground motion. In this paper, a novel damage index based on the monitoring of dynamic strain responses of steel beams under ambient vibration before and after earthquakes is firstly presented. Then, the relation between the amount of local damage and the presented damage index is derived numerically with a parametric study using a nine-story steel moment-resisting frame model designed for the SAC project. Finally, the effectiveness of the damage index and an associated wireless strain sensing system are examined with a series of vibration tests using a five-story steel frame testbed.

KEY WORDS: damage quantification; steel moment-resisting frames; dynamic strain; wireless sensing

1. INTRODUCTION

Knowing the location of damaged members and their extent of damage reduces uncertainty in evaluating the remaining capacity of earthquake-affected buildings and allows non-conservative decision-making on re-occupancy which may involve prioritized repairs. Nevertheless, the inspection of primary structural members, which are often covered with fire-proofing and architectural finishes, using non-destructive evaluation (NDE) techniques such as visual examination and ultrasonic testing require extensive costs and labors. Moreover, in the 1994 Northridge and 1995 Kobe earthquakes, where a large number of steel moment-resisting frames suffered fractures at welded beam-column connections [1, 2], while many damaged connections were discovered, a lot of connections that remained undamaged had to undergo inspection owing to apparent damage in concrete slabs or nonstructural elements around these connections.

46 Structural health monitoring (SHM), developed as a sophisticated technology for damage
47 identification, has the potential to provide rapid and reliable information about seismic damage in
48 a structure, and thus to avoid unnecessary inspections and downtime that hinder economic and
49 social recovery following a devastating earthquake. Using measured vibration responses, various
50 damage detection methods to date have been proposed, such as modal parameter-based method
51 [3], inter-story drift ratio-based method [4], seismic wave propagation method [5], and time
52 series analysis method [6]. At present, only a few important buildings located in earthquake-
53 prone regions have installed SHM systems as an extension of strong ground motion monitoring
54 systems in which the maximum floor responses and the changes in modal properties are primarily
55 utilized for estimating the damage of buildings [7, 8]. However, damage estimation based on the
56 global characteristics of buildings can only provide rough assessments due to large uncertainties
57 in the hysteresis behaviors of individual members and connections. They are hardly effective to
58 give reliable information for local damage on individual members (e.g., local buckling and
59 fracture in steel moment-resisting frames) as such local damage weakly relates to the global
60 characteristics of buildings. For example, through a series of shaking table testing in which
61 various levels of realistic seismic damage were reproduced for a high-rise steel building specimen
62 at the E-Defense facility in Japan, Ji *et al.* [9] demonstrated that the natural frequencies of the
63 specimen decreased by 4.1%, 5.4%, and 11.9% on average for three damage levels respectively,
64 while the mode shapes changed very little. The changes in the modal properties were largely
65 influenced by cracks in concrete slabs and barely provided the accurate location and extent of
66 seismic damage on individual steel members. Besides, through the same testing, Chung [10]
67 reported large variations in seismic damage at beam-column connections at the same floor level
68 that experienced nearly identical deformation.

69 As strain responses directly reflect the local information of the monitored structural members,
70 damage detection based on strain responses has drawn extensive attention to the health
71 monitoring of bridges, pipelines, and aircrafts in recent years. Li and Wu [11] and Hong *et al.* [12]
72 utilized long-gauge fiber Bragg grating (FBG) sensors to measure the strain distribution
73 throughout the full or critical areas of the Wayne bridge located in New Jersey in America under
74 ambient excitation and identified the location and extent of localized damage. Razi *et al.* [13]
75 reported a vibration-based damage detection strategy with strain information measured by lead
76 zirconate titanate (PZT) sensors for detecting bolt loosening of pipeline's bolted flange joints in
77 the oil and gas industry. Mujica *et al.* [14] located the position of impact damage on a section of a
78 commercial aircraft wing flap using strain responses sensed by PIC 155 (i.e., a modified PZT
79 material produced by PI Ceramic GmbH, Germany) piezoceramic sensors and a knowledge-
80 based reasoning methodology. Nevertheless, due to the high costs for the installation and
81 maintenance of the current tethered SHM systems, strain monitoring with a high-density
82 measurement system has been thought to be uneconomic and impractical in the building
83 engineering community. More importantly, as buildings are always excited by ambient vibrations
84 with large randomness, finding an effective strain-based damage index with independency of
85 external excitations for localized damage is a great challenge. Thus, research on the localized
86 damage detection of buildings with strain responses is very limited at present.

87 With the emergence of wireless sensing technology [15-17] and high-sensitivity piezoelectric
88 strain sensors [18], which have great potential to develop economical dense-array sensing
89 systems, Kurata *et al.* [19] developed a damage index based on the dynamic strain responses of
90 steel beams and verified its performance using a five-story steel frame testbed. Nonetheless, the
91 research only includes preliminary studies on damage detection and needs further generalization
92 in theoretical formulations and experimental studies for developing a damage quantification

methodology using dynamic strain information. This paper presents a general formulation of the damage index with dynamic strain responses. It is followed by studies on the influence of sensor location and input excitation on the damage index using a nine-story steel moment-resisting frame designed for the SAC project. To enable the quantification of local damage besides damage detection, the empirical curve for the relationship between the damage index and the reduction in bending stiffness at a fractured section was obtained for different sensor locations. Finally, the general formulation and the results of numerical studies were verified through a series of ambient vibration tests and shaking table tests using a five-story steel frame testbed.

2. DAMAGE INDEX FOR EVALUATING BEAM FRACTURE

2.1. Damage index based on changes of relative strain responses

In steel moment-resisting frames, inclusion of fracture at beam-ends changes the amplitude of the bending strain responses at the damaged beams, which are primarily influenced by the reduction in the bending stiffness of the damaged beams. Thus, a comparative study of the bending strain responses of beams for undamaged and damaged frames, which are excited with small dynamic loads (e.g., ambient vibrations and minor earthquake ground motions), allows the evaluation of the extent of damage to beams. In addition, adopting the equivalent static force approach [20] can eliminate the influence of external excitations on damage evaluation analysis. This section reformulates the strain-based damage evaluation methodology with bending strain responses, which was originally formulated with bending moment responses of beams in [19].

When an n -story steel moment-resisting frame is subject to lateral dynamic loads such as ground motions, at any instant of time t , the equivalent static forces $F(t) = [f_1(t), f_2(t), \dots, f_i(t), \dots, f_{n-1}(t), f_n(t)]^T$ act on the frame as external forces, as illustrated in Figure 1. Suppose the frame vibrates linearly under small-amplitude excitations, at instant of time t , a bending strain response measured at any beam can be formulated as

$$\varepsilon(t) = \alpha_1 f_1(t) + \alpha_2 f_2(t) + \dots + \alpha_i f_i(t) + \dots + \alpha_{n-1} f_{n-1}(t) + \alpha_n f_n(t) = \sum_{i=1}^n \alpha_i f_i(t), \quad (1)$$

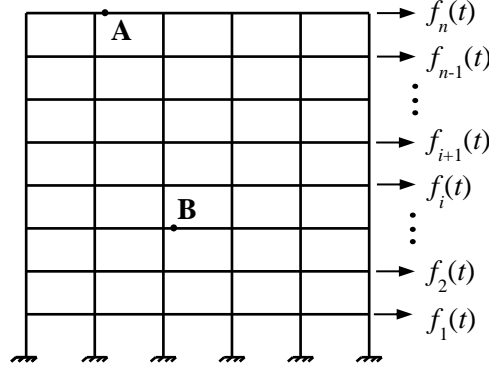
where α_i ($i = 1, \dots, n$) is an influence factor of the equivalent static force $f_i(t)$, which relates only to the structural properties (i.e., material and geometric properties) and is unaffected by the characteristics of external excitations. Since the equivalent static forces associated with the j th mode vibration are

$$F_j(t) = \omega_j^2 \mathbf{M} \Phi_j q_j(t), \quad (2)$$

the bending strain response of the beam associated with the j th mode is expressed as

$$\varepsilon_j(t) = \omega_j^2 q_j(t) \sum_{i=1}^n \alpha_i m_i \phi_{ij}, \quad (3)$$

135 where ω_j and $\Phi_j = [\phi_{1j}, \phi_{2j}, \dots, \phi_{ij}, \dots, \phi_{n-1j}, \phi_{nj}]^T$ are the j th modal frequency and mode shape;
 136 $\mathbf{M} = \text{diag}(m_1, m_2, \dots, m_i, \dots, m_{n-1}, m_n)$ is the mass matrix for the frame in which m_i ($i = 1, \dots, n$) is
 137 the lumped mass of the floor; and $q_j(t)$ is the modal coordinate for the j th mode [20].
 138



139 Figure 1. n -story steel moment-resisting frame under equivalent static forces.
 140

141 Now consider the ratio of the bending strain responses of beams associated with the j th mode
 142 at any two different positions A and B (position A as a reference point) at any instant time t :
 143

$$144 \quad \frac{\varepsilon_j^B(t)}{\varepsilon_j^A(t)} = \frac{\omega_j^2 q_j(t) \sum_{i=1}^n \alpha_i^B m_i \phi_{ij}}{\omega_j^2 q_j(t) \sum_{i=1}^n \alpha_i^A m_i \phi_{ij}} = \frac{\sum_{i=1}^n \alpha_i^B m_i \phi_{ij}}{\sum_{i=1}^n \alpha_i^A m_i \phi_{ij}} . \quad (4)$$

145
 146 The obtained ratio of the bending strain responses only relates to the structural properties of the
 147 frame, and has no relationship with external excitations. Reference point A needs to be located in
 148 the undamaged floor for evaluating the beam damage near point B. A floor with small
 149 deformation (e.g., the roof) is recommended for the reference point where the concrete slabs and
 150 beams at the floor remain undamaged. While not quantitatively examined, slight damage (i.e.,
 151 minor cracks in the concrete slabs and yielding of the beams) is deemed to have little influence
 152 on the bending strain at the reference point.

153 In practice, errors or uncertainties in data measurement and signal processing (e.g., time-
 154 synchronization errors, outliers, and distortion with filters) affect the instantaneous bending strain
 155 responses associated with the j th mode vibration, which are estimated as a peak in the frequency
 156 domain response, especially when the signal-to-noise (S/N) ratio is not large with small-
 157 amplitude excitations. Therefore, given the bending strain time histories with a time interval of Δt
 158 (each including k points) at two positions A and B, the ratio of the root mean square (RMS) of
 159 these two time histories under the j th mode vibration is considered as
 160

$$\frac{(\varepsilon_j^B)_{RMS}}{(\varepsilon_j^A)_{RMS}} = \frac{\sqrt{\frac{1}{k} \sum_{p=0}^{p=k-1} [\varepsilon_j^B(p\Delta t)]^2}}{\sqrt{\frac{1}{k} \sum_{p=0}^{p=k-1} [\varepsilon_j^A(p\Delta t)]^2}} = \frac{\sqrt{\frac{1}{k} \left(\omega_j^2 \sum_{i=1}^n \alpha_i^B m_i \phi_{ij} \right)^2 \sum_{p=0}^{p=k-1} [q_j(p\Delta t)]^2}}{\sqrt{\frac{1}{k} \left(\omega_j^2 \sum_{i=1}^n \alpha_i^A m_i \phi_{ij} \right)^2 \sum_{p=0}^{p=k-1} [q_j(p\Delta t)]^2}} = \frac{\sum_{i=1}^n \alpha_i^B m_i \phi_{ij}}{\sum_{i=1}^n \alpha_i^A m_i \phi_{ij}}. \quad (5)$$

162 The RMS ratio for the two bending strain time histories in Equation (5) equals the instantaneous
 163 relative bending strain in Equation (4) if there are no errors or uncertainties.

164 Two strain sensors S1 and S2 are placed on the bottom flanges of beams at positions A and B
 165 in Figure 1, respectively, to detect seismic damage at beam-end near position B. S1 is used as a
 166 reference sensor, which is sufficiently far from the damaged beams in the frame and unaffected
 167 by the damage. S2 is near the damage as a detecting sensor. In the undamaged condition, the
 168 relative RMS value of the bending strain time histories at the two sensors S1 and S2 associated
 169 with the j th mode is expressed as
 170

$$R_j = \frac{(\varepsilon_j^{S2})_{RMS}}{(\varepsilon_j^{S1})_{RMS}} = \frac{\sum_{i=1}^n \alpha_i^{S2} m_i \phi_{ij}}{\sum_{i=1}^n \alpha_i^{S1} m_i \phi_{ij}}, \quad (6)$$

173 while under the damaged condition, it is expressed as
 174

$$R_j^d = \frac{(\bar{\varepsilon}_j^{S2})_{RMS}}{(\bar{\varepsilon}_j^{S1})_{RMS}} = \frac{\sum_{i=1}^n \bar{\alpha}_i^{S2} m_i \bar{\phi}_{ij}}{\sum_{i=1}^n \bar{\alpha}_i^{S1} m_i \bar{\phi}_{ij}}, \quad (7)$$

177 where the variables with top bars are for the damaged condition. Finally, the damage index DI
 178 based on the bending strain responses of beams for detecting seismic damage on beams in steel
 179 moment-resisting frames can be defined as follows
 180

$$DI = \frac{R_j^d - R_j}{R_j} \times 100\%. \quad (8)$$

183 where if $R_j^d = R_j$, i.e., no damage, DI is 0; if $R_j^d = 0$, i.e., complete fracture, DI is -100% .

184 Note that fracture at beam-ends has two influential factors on the bending strain responses
 185 measured by S2: (1) the bending strain decreases because of the reduction in the bending moment
 186 resisted by the damaged beam; and (2) the bending strain is affected by local strain redistribution
 187 around the fractured section. If sensor S2 is located in the region unaffected by the local strain
 188 redistribution, DI is proportional to the reduction of the bending moment.
 189

190 2.2. Signal processing for damage estimation

192

193 Figure 2 shows a step-by-step procedure for calculating the damage index DI . First, raw dynamic
 194 strain data of steel beams is preprocessed with data cleaning techniques (e.g., the removal of
 195 drifts and false points). Second, one mode of the steel moment-resisting frame is selected and the
 196 strain responses associated with the selected mode are extracted using band-pass filters. Third,
 197 the RMS values of the filtered strain data are calculated and then normalized by the RMS value
 198 of a reference position. Finally, damage information (existence, location, and extent) is extracted
 199 from the damage index DI calculated in Equation (8) at each detecting sensor.
 200

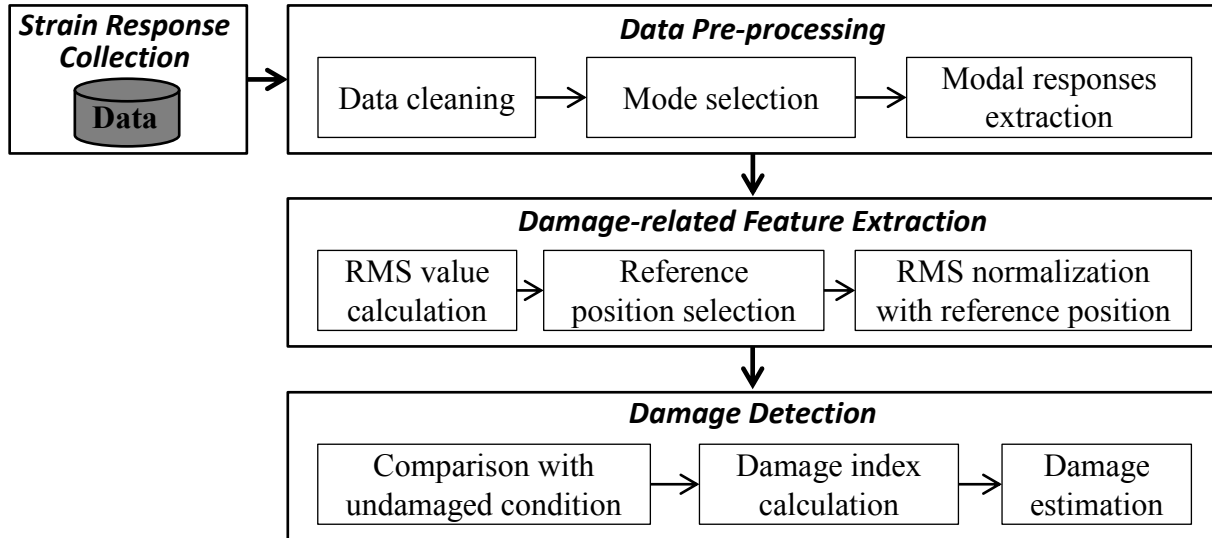


Figure 2. Procedure of damage evaluation.

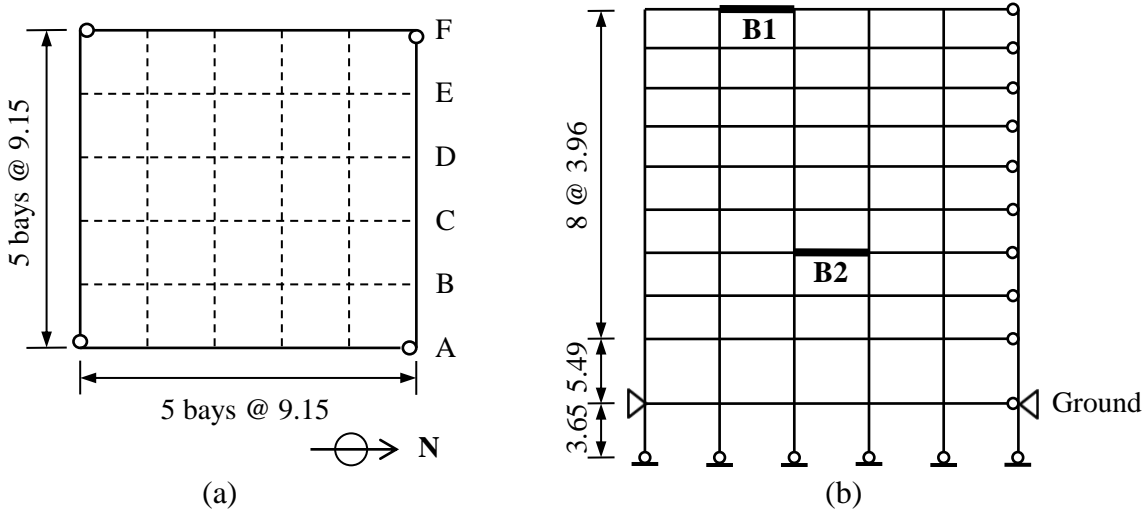
201
 202
 203
 204
 205
 206
 207
 208
 209

3. NUMERICAL ANALYSIS WITH A NINE-STORY STEEL MOMENT-RESISTING FRAME

3.1. Nine-story building model

210 The effectiveness of the presented damage index DI in evaluating the damage extent of seismic
 211 fracture on steel beams was verified through a numerical case study using the LA pre-Northridge
 212 nine-story building intensively studied in the SAC steel project [21]. The nine-story building
 213 represents typical medium-rise buildings designed according to the pre-Northridge design
 214 practice in Los Angeles, California. The building is 45.73 m by 45.73 m in plan, and 37.19 m in
 215 elevation (see Figure 3). Each bay spans 9.15 m in both the N-S and E-W directions. The lateral
 216 load-resisting system of the building comprises four perimeter steel moment-resisting frames.
 217 The interior bays of the structure contain gravity frames with composite floors. The wide flange
 218 columns of the moment-resisting frames are made from 345 MPa steel. The column bases are
 219 modeled as pin connections. The horizontal displacement of the structure at ground level is
 220 assumed to be restrained. The floor system consists of wide flange beams made of 248 MPa steel
 221 acting compositely with floor slabs. Typical beam sizes are W36x160 (with I_x of 4.062×10^9
 222 mm^4) from the ground to the third floors, W36x135 (with I_x of 3.247×10^9 mm^4) from the fourth
 223 to seventh floors, and smaller beam sizes for the upper levels. The inertial effects of each floor
 224 are assumed to be evenly carried by each perimeter moment-resisting frame through the floor
 225 system. Hence, each frame resists one half of the seismic mass. The seismic mass of the ground

226 level is 9.65×10^5 kg, for the second floor is 1.01×10^6 kg, for the third through ninth floors is
 227 9.89×10^5 kg, and for the tenth floor is 1.07×10^6 kg.
 228



229 Figure 3. SAC nine-story building (unit: m): (a) building plan; (b) frame A elevation.

230
 231
 232

3.2. Numerical simulation model

233 The numerical study was conducted using the finite element (FE) analysis software, Marc [22].
 234 Seismic fracture on one beam with various levels of damage extent was considered to verify the
 235 effectiveness of the presented damage index. The relation between the damage index and the
 236 location of strain sensors on a beam was also studied. As most seismic-induced beam fractures
 237 begin at the toe of the weld access hole and extend to the web, the beam fracture was simulated
 238 by cutting the bottom flange and/or web near the column surface at the left end of beam B2
 239 (Figure 4). The length of the cut was one percent of the beam length. There were seven damage
 240 patterns for beam seismic fracture simulation, as listed in Table 1. DP1 to DP3 simulated fracture
 241 at one side of the bottom flange, where the decreases of the bending stiffness EI_x at the cut
 242 section were smaller than 22%. DP4 simulated the entire bottom flange fracture, in which the
 243 bending stiffness EI_x at the cut section decreased by 49%. Severe fracture damage extending from
 244 the bottom flange to the web was simulated in DP5 to DP7 with the reduction of more than 75%
 245 in the bending stiffness EI_x at the cut section. In the finite element model, two beams B1 and B2
 246 were modeled with shell elements, and other beams and columns were modeled with beam
 247 elements (Figure 5). The nodes of shell elements at the beam-ends were connected to the nodes of
 248 beam elements with rigid links.

249 The measurement locations of the bending strain responses of beams are shown in Figure 6.
 250 S_{ref} as a reference sensor was set on the left end of beam B1 at the top floor where was considered
 251 to be far from the damage location (Figure 6(a)). In practice, several beams with the least damage
 252 probability may be selected to set reference sensors. S1 to S8 as detecting sensors were on one
 253 side of the bottom flange of beam B2 at intervals of l or $2l$ ($l = 0.2d_2$, where d_2 is the depth of
 254 beam B2) from the column surface (Figure 6(b)). The frame was excited with two excitations
 255 (Figure 7): (1) a white noise (WN); and (2) an earthquake ground motion (EM).
 256

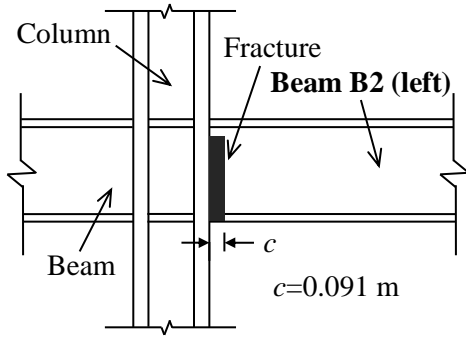


Figure 4. Simulated fracture.

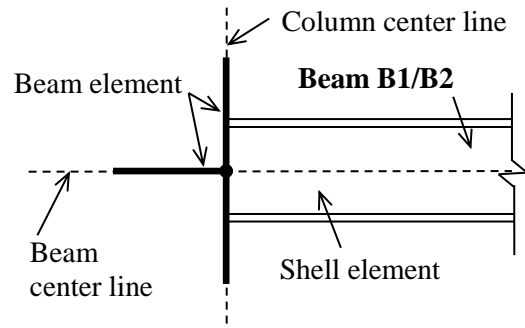


Figure 5. Connection between beam elements and shell elements.

257
258

Table 1. Damage patterns for fracture simulation.

Damage pattern	Undamaged	DP1	DP2	DP3	DP4
Cross-section					
EI_x reduction (%)	0	6.5	13.5	21.2	49.1
Damage pattern	DP5	DP6	DP7		
Cross-section					
EI_x reduction (%)	76.1	91.8	98.7		

259

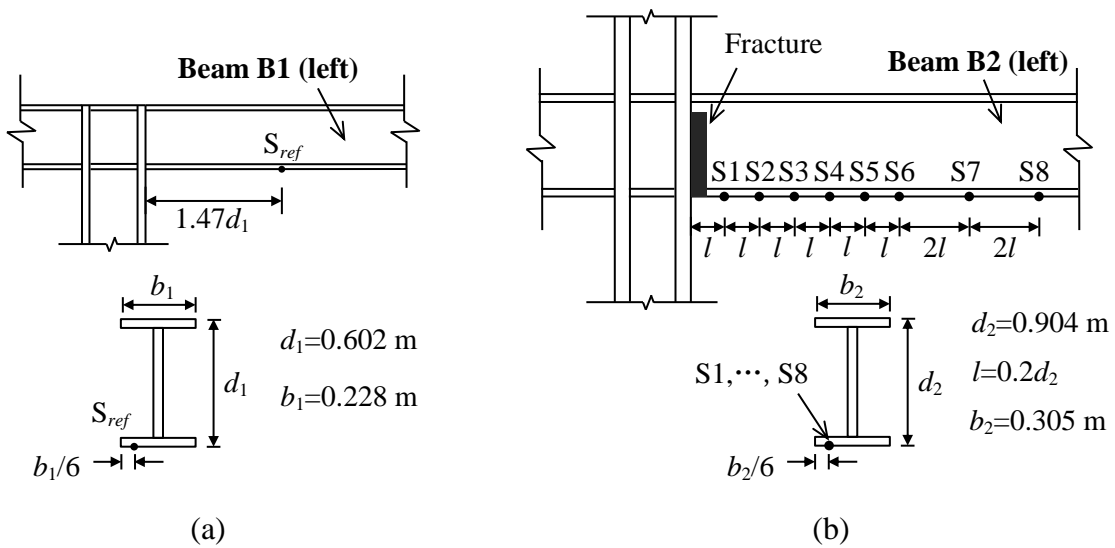


Figure 6. Strain output location: (a) reference sensor; (b) detecting sensors.

260
261

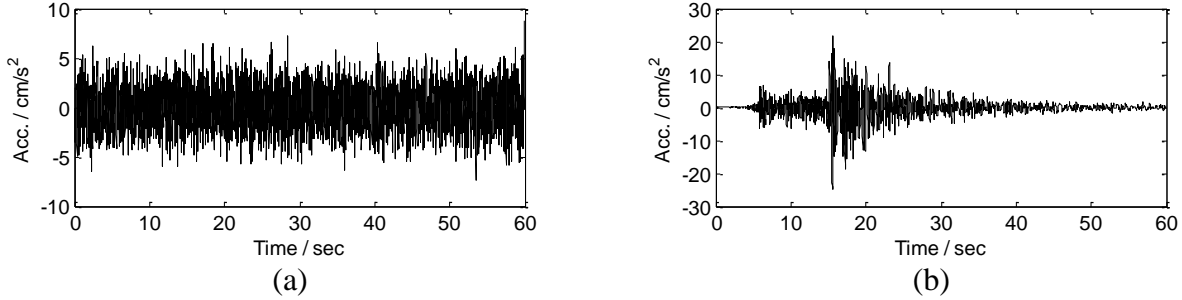


Figure 7. Input excitations: (a) white noise; (b) earthquake ground motion.

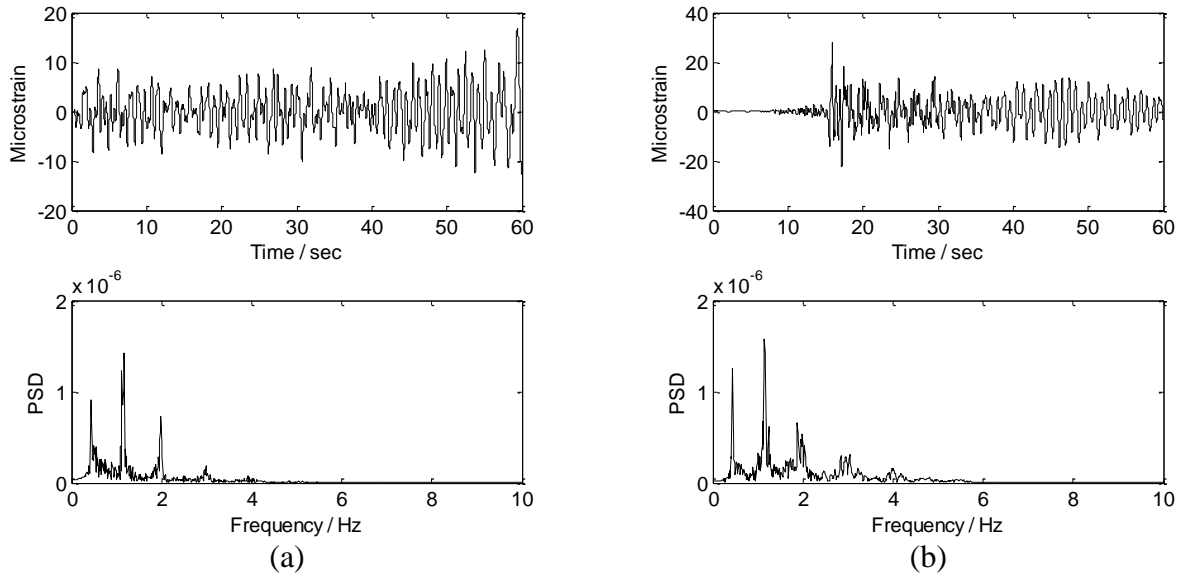
262
263

264 3.3. Data preprocessing

265

266 The first four natural frequencies of the undamaged model of the nine-story frame were 0.432,
267 1.150, 1.987, and 2.988 Hz, which were consistent with those reported previously [23]. For
268 reference, the inclusion of the severest damage condition at Beam B2 (DP7 with a reduction of 99%
269 in the bending stiffness EI_x at the cut section) reduced the first four natural frequencies to 0.429,
270 1.150, 1.980, and 2.963 Hz, where the largest change in these frequencies was only 0.9%. Note
271 that damage to a critical member that assures the overall stability of the frame, such as a column,
272 can lead to a more significant change in the natural frequency.

273 Figure 8 shows the bending strain responses and their power spectral densities of the reference
274 sensor S_{ref} at the undamaged condition. The power spectral densities (PSD) for both excitations
275 indicate that the responses of the frame were mainly dominated by the first three modes.
276 Therefore, the bending strain responses associated with the first three modes were respectively
277 used to calculate the damage index DI . The strain responses associated with each mode were
278 obtained using band-pass filters on raw strain responses. Considering the slight changes in the
279 natural frequencies with the inclusion of damage, the bandwidth of the band-pass filter was set to
280 include $\pm 10\%$ of each natural frequency. Thus, the band-pass filters were 0.38-0.48, 1.04-1.27,
281 and 1.79-2.19 Hz for the first three modes.



282 Figure 8. Bending strain responses at reference sensor S_{ref} : (a) white noise; (b) earthquake ground
283 motion.

284

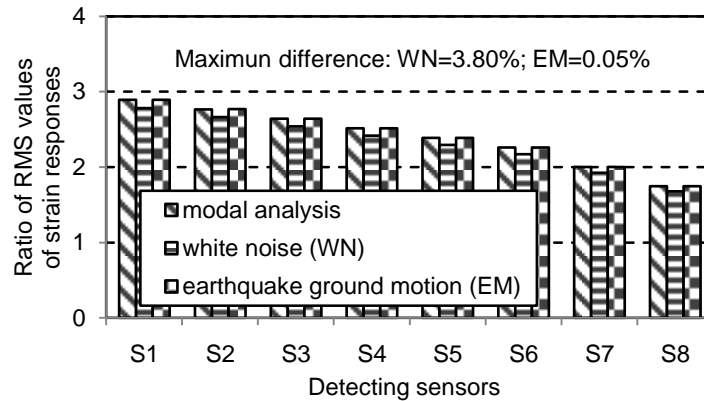
285 3.4. Simulation results

286

287 3.4.1 Independency on excitations and modes

288

289 The variations in the ratio of RMS values of the bending strain responses were studied for the
 290 undamaged condition. Figure 9 shows the ratios of the first mode for each detecting sensor (i.e.,
 291 S1 to S8) relative to the reference sensor S_{ref} . The values of the ratio were the largest at S1 and
 292 the smallest at S8, and proportional to the bending moments sustained at each beam section.
 293 When two excitations were compared using modal analysis (i.e., no need to extract the modal
 294 strain responses from the time histories), the difference was up to 3.8% for the white noise, and
 295 0.05% for the earthquake ground motion, which confirmed the independence of the extracted
 296 ratio of RMS values on external excitation as indicated by Equation (5) of the preceding
 297 theoretical formulation. Note that the differences arise from errors in the extraction of the modal
 298 strain responses with band-pass filters. Compared to the white noise, the earthquake ground
 299 motion that generated a relatively large-amplitude strain response (see Figure 8) had a small
 300 discrepancy.
 301



302

302 Figure 9. Ratio of RMS values for different detecting sensors and excitations.

303

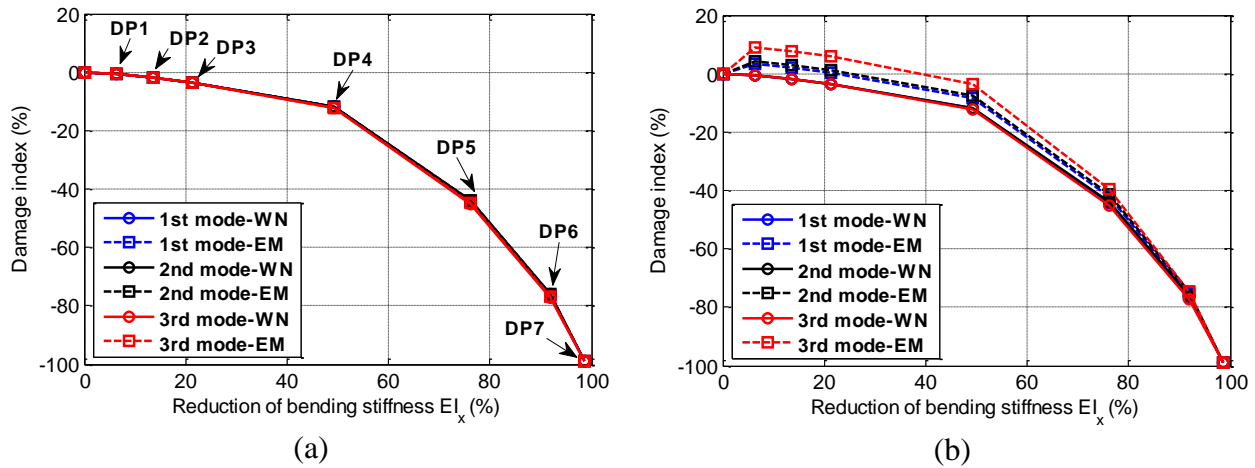
304 Next, the selection of reference values and modes were studied. Figure 10 shows the damage
 305 index DI at sensor S6 for two different selections of the reference values under the undamaged
 306 condition.

307 *Reference 1:* Ideal case where the same excitation was used for undamaged and damaged
 308 conditions.

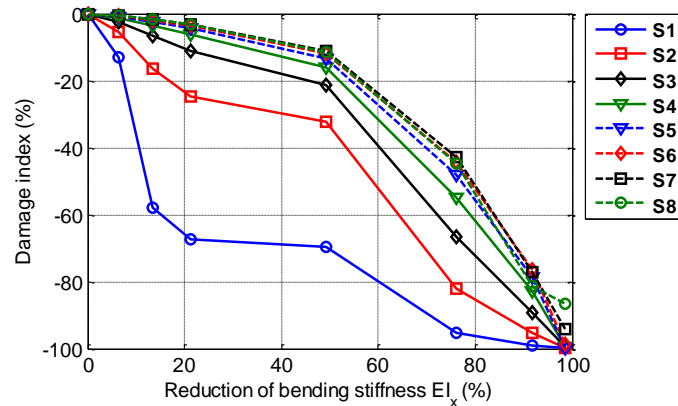
309 *Reference 2:* Practical case where ambient vibration assumed to be white noise was used to
 310 prepare the reference values under the undamaged condition.

311 The horizontal axes of the plots are the reduction of the bending stiffness at the fractured
 312 section and the vertical axes are the damage index DI calculated with Equation (8). As the
 313 bending stiffness EI_x decreases, the damage index drops from 0 to -100% . When reference 1 was
 314 applied, the damage indices were identical for different excitations and selected modes. In
 315 contrast, when reference 2 was applied, while the damage indices extracted from strain responses
 316 under white noise were identical for the first three modes, the damage indices extracted from the
 317 strain responses under earthquake ground motion contained errors (as the errors significantly
 318 exceeded the real damage index at DP1 to DP3, the damage index takes positive values that are

319 false-negative). This is because the errors in the extraction of modal responses with band-pass
 320 filters under the undamaged and damaged conditions were not identically offset. The maximum
 321 error of the damage indices extracted from the first two modes was not greater than 4%, while
 322 that for the third mode without a clear fundamental peak (see Figure 8(b)) exceeded 9%. In
 323 Figure 8(b), the power ratio of the fundamental peak to the irrelevant noise (i.e., responses not
 324 related to the natural vibration modes) in the filter bandwidth is 64.1 dB for the first mode, 2.1
 325 dB for the second mode, and 0.3 dB for the third mode. In summary, the dominant modes with a
 326 higher peak in the power spectral density are more suitable for computing the damage index.
 327



328 Figure 10. Damage index DI at detecting sensor $S6$: (a) with the first selection of reference
 329 values; (b) with the second selection of reference values.
 330



331
 332 Figure 11. Damage index at all detecting sensors $S1$ to $S8$.
 333

334 3.4.2 Influence of sensor location

335
 336 As mentioned in section 2, strain responses near beam-ends are influenced by local strain
 337 redistributions around fractures. Thus, the transition of the damage index along the beam axis
 338 was studied. According to the finding in the preceding section, the damage index was extracted
 339 from the first mode vibration under white noise excitation and with reference 1. Figure 11 shows
 340 the damage index for all detecting sensors $S1$ to $S8$. The damage index was affected by the local
 341 strain redistribution at $S1$ to $S5$ (i.e., the region that is less than $1.2d$ from the column surface). In
 342 contrast, the damage index was almost identical at $S6$ to $S8$ (i.e., the region that is more than $1.2d$

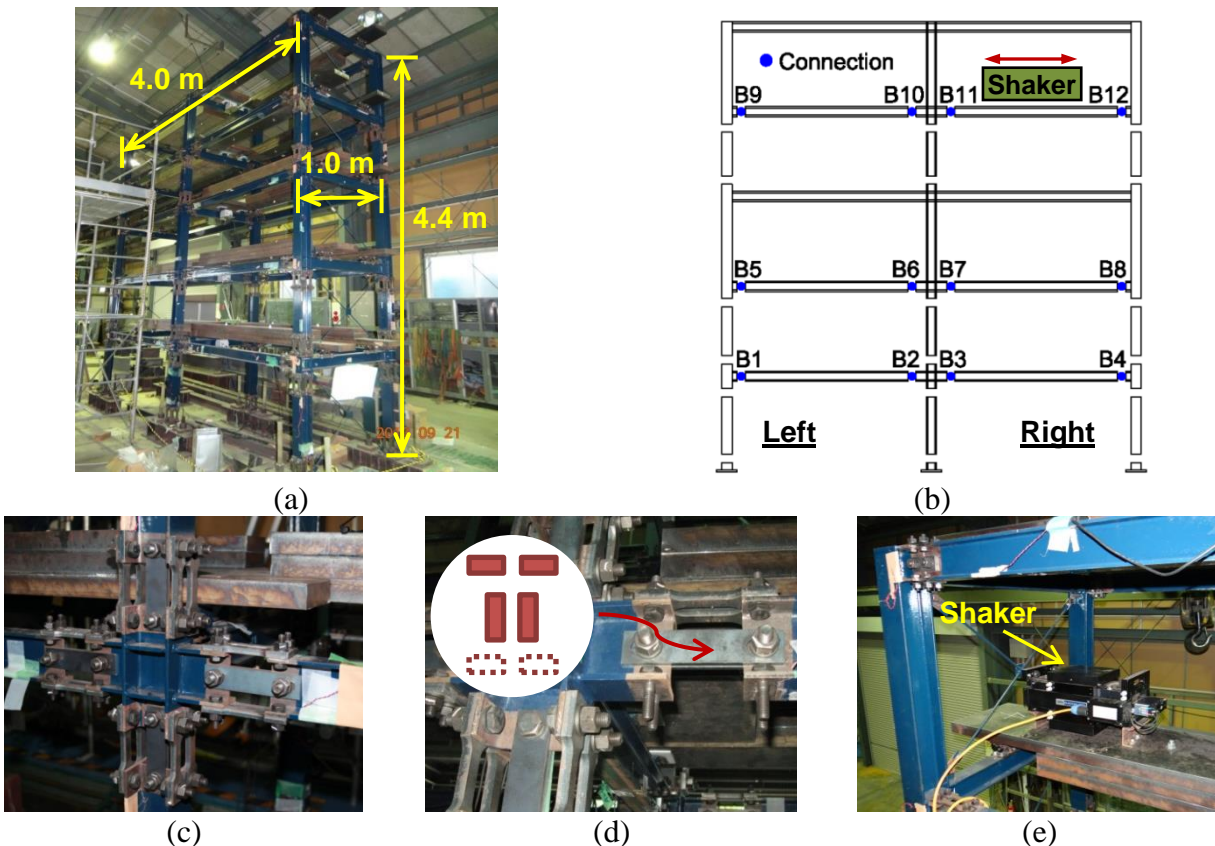
343 from the column surface), which indicates that the influence of the local strain redistribution is
 344 negligible and the values of the damage index are related primarily to the extent of moment
 345 redistribution induced by the damage.

346 Practically speaking, as the beam-end region within one beam depth from column surfaces
 347 may sustain large plastic deformation during strong earthquake events, detecting sensors had
 348 better be placed outside that region to be fully functional after the events. Thereby, it is
 349 recommended to place damage-detecting sensors at a distance of larger than $1.2d$ from the
 350 column surface, and to estimate the reduction in the bending stiffness at the fractured section with
 351 the empirical curve shown in Figure 11.

352 353 354 4. EXPERIMENTAL VERIFICATION USING A FIVE-STORY STEEL FRAME 355 TESTBED

357 A series of vibration tests was conducted to experimentally verify the presented damage index. A
 358 quarter-scale five-story steel moment-resisting frame constructed in the structural laboratory at
 359 the Disaster Prevention Research Institute (DPRI), Kyoto University, was used as the testbed
 360 frame. In the tests, a wireless strain sensing system was used to measure the bending strain
 361 responses of steel beams.

362



363 Figure 12. Steel frame testbed: (a) overview; (b) beam removable connections; (c) beam-column
 364 connection; (d) simulated damage; (e) modal shaker.

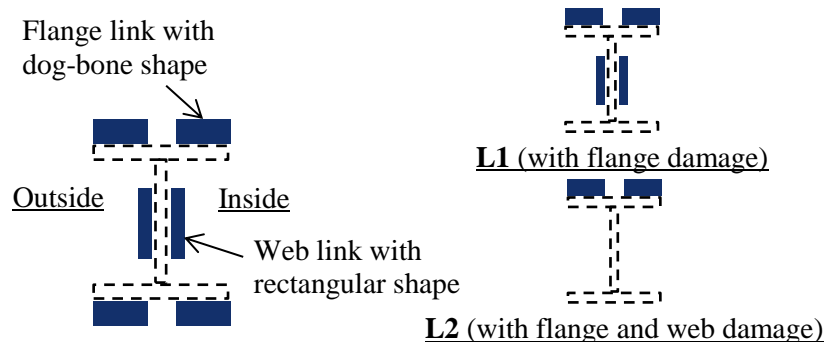
365

366 4.1. Steel frame testbed

367
 368 The overall dimensions of the steel frame were $1.0 \times 4.0 \times 4.4$ m (Figure 12(a)). The plan of the
 369 frame was one bay by two bays. At the second, third and fifth floors, beams in the longitudinal
 370 direction and columns were connected to joints using removable steel connections (four links at
 371 the flanges and one pair of links at the web) (Figure 12(b and c)). By removing the links, fracture
 372 damage was simulated (see Figure 12(d)). The five-story steel frame testbed was described in
 373 detail by Kurata *et al.* [19].

374 375 4.2. Damage patterns

376
 377 Considering typical fracture patterns of wide flange beams in steel buildings, which initiated
 378 from the tail of weld access holes at bottom flanges, two types of fracture damage, i.e., fracture of
 379 the bottom flange and web, were simulated. Figure 13 illustrates the cross-section of the
 380 removable connection and two levels of simulated fracture damage. In damage level 1 (L1), two
 381 links of the bottom flange of the connection were removed. In damage level 2 (L2), both bottom
 382 flange and web links were removed. As summarized in Table 2, the reduction in the bending
 383 stiffness about the strong axis of the beam section was 68.5% for damage L1 and 99.8% for
 384 damage L2.



386
 387
 388 Figure 13. Damage patterns.

Table 2. Damage categories.

Damage category	Description	Reduction of EI_x (%)
L1	All links of bottom flange are removed	68.5
L2	All links of bottom flange and web are removed	99.8

389 390 4.3. Damage cases

391
 392 In the testbed frame, there are twelve removable beam connections, connections B1 to B12 (see
 393 Figure 12(b)), in each longitudinal frame. Three different types of vibration test (i.e., Test 1 to
 394 Test 3) including a total of ten damage cases were conducted to evaluate the performance of the
 395 damage index and to verify the findings of the previous numerical simulations on input
 396 excitations and sensor locations.

397 *Test 1:* Independency of the damage index on external excitations and vibration modes was
 398 verified with a shaking table at the DPRI as excitation source. Damage L1 and L2 were
 399 simulated at connection B2 near the inner joint of the second floor.

400 *Test 2:* Influence of sensor location on the damage index was examined with a modal shaker as
 401 excitation source. Damage L1 and L2 were simulated at connection B1 near the exterior joint
 402 of the second floor.

403 *Test 3:* General applicability of the damage index was examined with a modal shaker as
 404 excitation source. Two levels of fracture damage, Damage L1 and L2, were simulated at three
 405 different connections B2, B6, and B10.

406 *Test 4:* Influence of neighboring damage on the damage index was studied with a modal
 407 shaker as excitation source. As beam seismic damage changes the moment distribution rather
 408 locally, only the influence of fracture damage at the closest beam-ends on the same floor level
 409 was considered.

410 Test 4 was conducted to obtain preliminary data for multiple damage condition; at this
 411 moment, the presented damage index does not explicitly consider the influence of neighboring
 412 damage and further study is required. Note that all the tests considered fracture damage only in
 413 one longitudinal frame, while another longitudinal frame remained intact. The inclusion of
 414 asymmetric damage may induce torsional vibrations of the frame but the influence on the lateral
 415 mode vibrations was found negligible.

416

417

Table 3. Damage cases.

Test	Damage Case	Damage				Targets	Loading system
		As detected		Influence sources			
		Location	Category	Location	Category		
Test 1	Undamaged	-	-	-	-	Independency on excitations and modes	Shaking table
	Case 1	B2	L1	-	-		
	Case 2	B2	L2	-	-		
Test 2	Case 3	B1	L1	-	-	Influence of sensor location	Modal shaker
	Case 4	B1	L2	-	-		
Test 3	Case 5	B2	L1	-	-	General applicability	Modal shaker
	Case 6	B6	L1	-	-		
	Case 7	B10	L1	-	-		
	Case 8	B2	L2	-	-		
	Case 9	B6	L2	-	-		
Test 4	Case 10	B10	L2	-	-	Influence of neighboring damage	Modal shaker
	Case 11	B3	L1	-	-		
	Case 12	B3	L1	B2	L1		
	Case 13	B3	L1	B2	L2		
	Case 14	B3	L1	B4	L2		
	Case 15	B3	L2	-	-		
	Case 16	B3	L2	B2	L2		
Case 17	B3	L2	B4	L2			

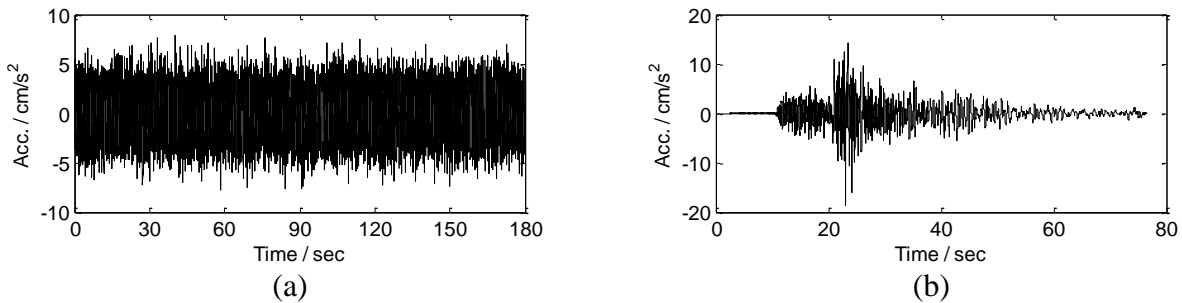
418

419 *4.4. Excitations*

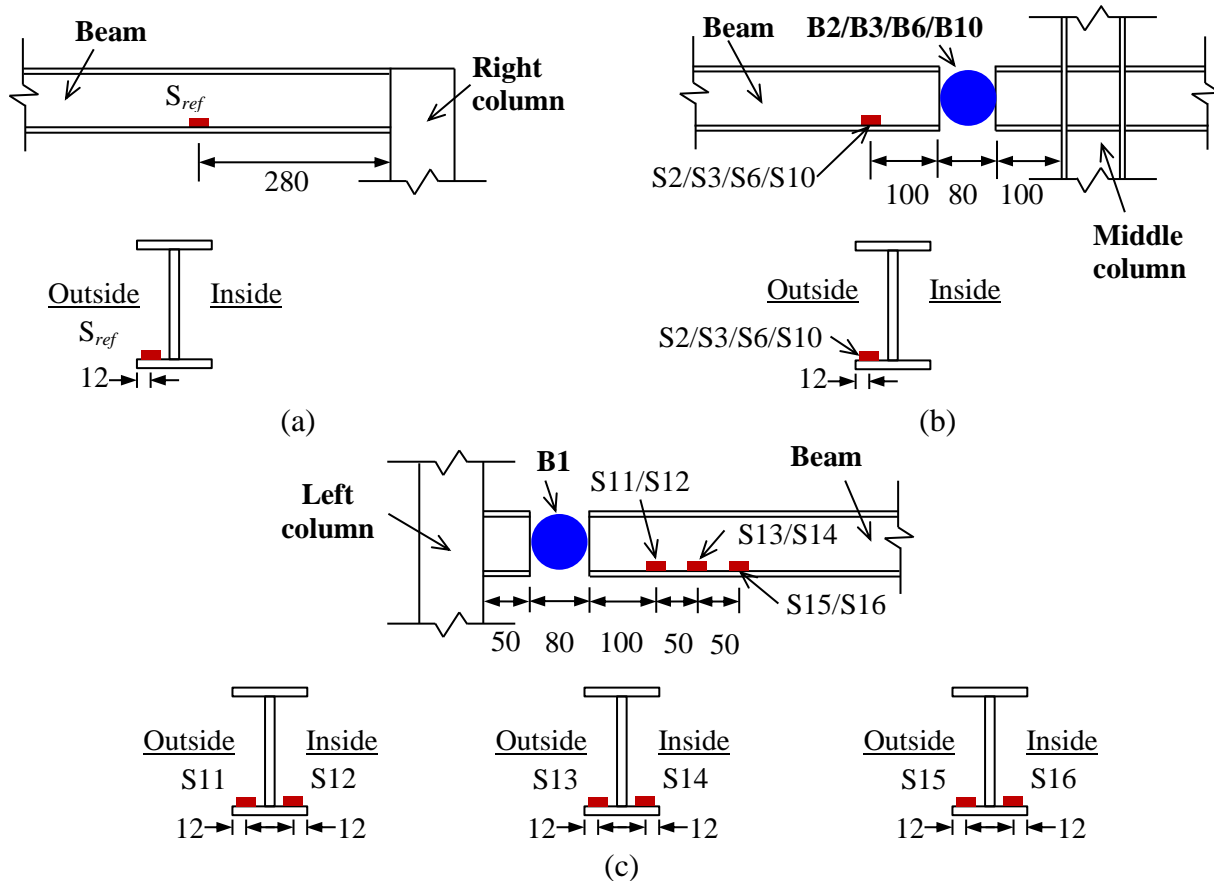
420

421 In Test 1, the steel frame was excited in the longitudinal direction by the shaking table at the
 422 DPRI, Kyoto University, with two small-amplitude excitations (Figure 14): (1) a white noise
 423 (WN) with a frequency range of 1 to 50 Hz and RMS of 2 cm/s²; and (2) an small-amplitude
 424 earthquake ground motion (EM) with the maximum acceleration of 18 cm/s². In the undamaged

425 frame, these excitations induced the top floor acceleration responses of 4.38 and 12.32 cm/s² in
 426 RMS, respectively. In Tests 2, 3 and 4, the steel frame testbed was excited at the fifth floor using
 427 a modal shaker (APS-113, APS Dynamics) firmly fixed to the steel mass plate (Figure 12(e)).
 428 The steel frame was excited in the longitudinal direction using three excitations: (1) ambient
 429 excitation (AmbE); (2) small-amplitude white noise with a frequency range of 1 to 50 Hz (WN1);
 430 and (3) relatively large-amplitude white noise with a frequency range of 1 to 50 Hz (WN2). In the
 431 structural laboratory where the testbed frame was located, ambient vibrations mainly caused by
 432 ground microtremor was around 0.49 cm/s² in RMS at the top floor. When the undamaged frame
 433 was excited with two white noise excitations, the roof acceleration responses were 3.32 and 8.45
 434 cm/s² in RMS for WN1 and WN2, respectively.
 435



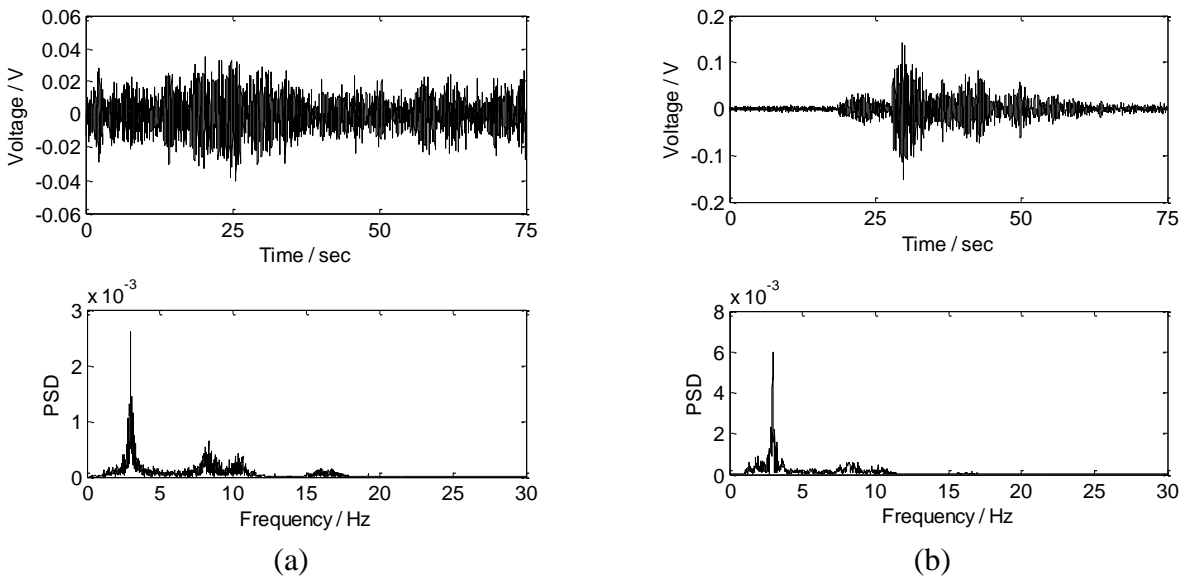
436 Figure 14. Input excitations for the shaking table: (a) white noise; (b) earthquake ground motion.
 437



438 Figure 15. PVDF sensor location (unit: mm): (a) reference sensor; (b) sensors in Tests 1, 3 and 4;
 439 (c) sensors in Test 2.

440
 441 *4.5. Sensor location*
 442

443 Polyvinylidene difluoride (PVDF) piezo films (DT1-028K/L, Measurement Specialties, USA)
 444 [24] interfaced with *Narada* wireless sensing units (Civionics, LLC, USA) [25] were used in the
 445 tests. In all tests, the reference sensor S_{ref} (Figure 15(a)) was placed at the top floor. In Tests 1, 3
 446 and 4, detecting sensors were placed on one side of the beam bottom flange at $1.0d$ (the beam
 447 depth d is 100 mm) away from the edge of the fracture, as illustrated in Figure 15(b). Sensors S2,
 448 S3, S6, and S10 were used to detect the simulated damage at connections B2, B3, B6, and B10
 449 respectively. In Test 2, detecting sensors were attached on both sides of the beam bottom flange
 450 at $1.0d$, $1.5d$, and $2.0d$ away from the edge of the fracture to examine the influence of sensor
 451 location. Six sensors S11 to S16 used to detect the damage at connection B1 are shown in Figure
 452 15(c). While not included in this paper, when the fracture progressed from the tail of the weld
 453 access hole asymmetrically about the beam axis (e.g., the fracture of half of the bottom flange),
 454 the amount of local strain redistribution differed at each side of the bottom flange. Nevertheless,
 455 the influence of local strain redistribution was expected to disappear at a sufficient distance from
 456 the fractured section.
 457



458 Figure 16. Measured signals at S_{ref} in Test 1: (a) white noise; (b) earthquake ground motion.
 459

460 *4.6. Results and discussions*
 461

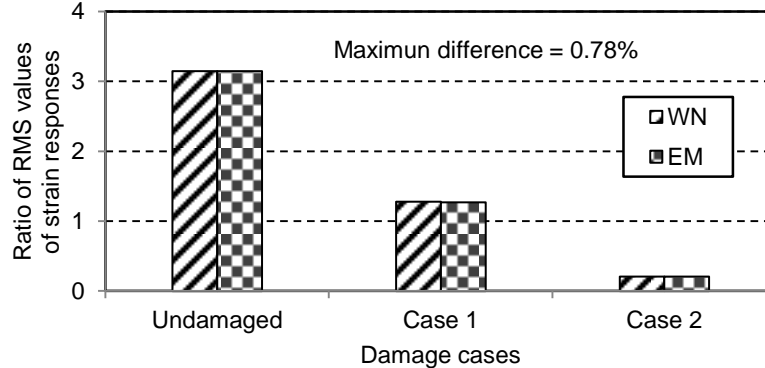
462 In all tests, bending strain responses were recorded for 75 seconds with the sampling rate of 100
 463 Hz. Figure 16 shows the strain responses in voltage units (one microstrain corresponds
 464 approximately to 12 mV) and their power spectral densities at the reference sensor S_{ref} for two
 465 excitations, which were measured from the undamaged condition in the shaking table tests of
 466 Test 1. The power spectral densities indicated that the structural vibration was mainly dominated
 467 by the first mode. The first two natural frequencies of the testbed frame were 3.16 and 8.33 Hz
 468 for the undamaged condition, 3.11 and 8.25 Hz for Case 2, and 3.05 and 8.31 Hz for Case 17.

469 Note that Case 17 was one of serious damage cases among all considered damage cases. The
 470 band-pass filter of 2.70-3.30 and 7.40-9.20 Hz ($\pm 10\%$ of the natural frequencies at the
 471 undamaged condition as the band width) were used to obtain the modal strain responses of the
 472 first two modes. The averaged ratio of RMS values for different excitations at the undamaged
 473 condition were used as the reference values.

474 475 4.6.1. Test 1

476
477 Figure 17 shows the ratios of RMS values of strain responses between sensor S2 and reference
 478 sensor S_{ref} for the first mode. The largest difference in the ratio values between the two different
 479 excitations was 0.78%, which verified independency of the extracted ratio on external excitations
 480 as observed in the preceding theoretical formulation and numerical simulations.

481 The damage indices of sensor S2 for detecting damage L1 and L2 at connection B2 are
 482 summarized in Table 4. In Case 1 with damage L1, i.e., entire bottom flange fracture with the
 483 reduction of 68.5% in the bending stiffness, the damage indices were about -60% for both
 484 excitations with the use of the first mode vibrations but changed to -70% with the use of the
 485 second mode vibrations. Compared to the damage index extracted from the first mode, the
 486 damage index of the second mode had larger discrepancy as the modal strain responses were
 487 weak and unclear (see Figure 16). In Case 2 with damage L2, i.e., entire bottom flange and web
 488 fracture with the decrease of 99.8% in the bending stiffness, the damage indices were smaller
 489 than -90% for two excitations with the first mode vibrations and slightly decreased with the
 490 second mode vibrations. As a result, the dominant modes with clear modal responses and high
 491 power are highly desirable to increase the accuracy of the calculation of damage index.



492
493 Figure 17. Ratio of RMS of strain responses at S2 and S_{ref} for the first mode in Test 1.

494
495 Table 4. Damage index for detecting damage at connection B2 in Test 1.

Mode	Excitation	Damage index (%)		
		Undamaged	Case 1	Case 2
1st mode	WN	0.0	-59.5	-93.5
	EM	0.0	-59.7	-93.4
2nd mode	WN	-1.0	-68.9	-96.5
	EM	1.0	-68.4	-96.7

496 497 4.6.2. Test 2

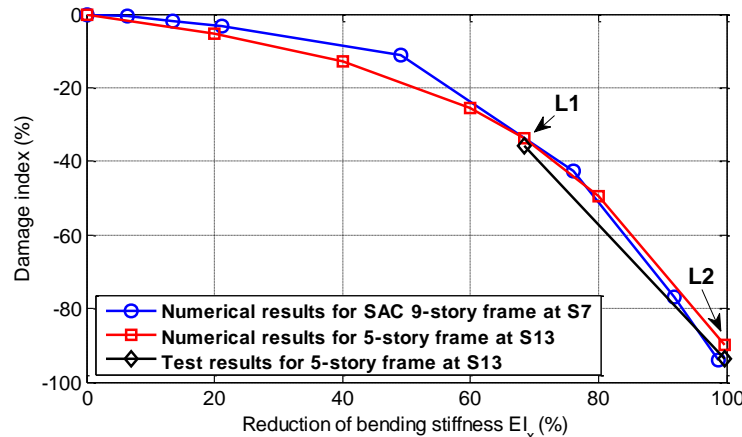
498

499 Table 5 summarizes the results of Test 2 for different sensor locations. When damage L1 was
 500 considered at connection B1 in Case 3, the damage indices at sensors S11 and S12, both placed at
 501 100 mm (i.e., the beam depth) away from the edge of the fracture, were about -50% , whereas the
 502 damage indices at sensors S13 and S14, both at 150 mm (i.e., one and half beam depths) away
 503 from the edge, were around -35% to -37% . The damage indices at sensors S15 and S16, both
 504 attached at 200 mm (i.e., two beam depths) away from the edge, were -32% to -36% and
 505 consistent with those at S13 and S14. When damage L2 was considered at connection B1 in Case
 506 4, the damage index at the six sensors S11 to S16 was less than -85% . Compared to the damage
 507 index of about -95% at sensors S11 and S12, the damage index at sensors S13 to S16 had slight
 508 changes of 10% , which was consistent with the findings in the preceding numerical simulations
 509 for severe damage DP7; strain sensors needed to be set within two beam depths to guarantee the
 510 monotonic relation between the damage index and the reduction of bending stiffness. Note that
 511 the values at the different sides of the flange (e.g., S13 and S14, and S15 and S16) varied by 5%
 512 with beam torsional vibrations observed when web links were removed. In conclusion, in order to
 513 obtain a stable relation between the damage index and the reduction of bending stiffness, like the
 514 damage index curves for sensors S6 to S8 in Figure 11, detecting sensors need to be placed with
 515 the distance of at least $1.5d$ but no farther than $2.0d$ from fracture damage as recommended by the
 516 previous simulations using the SAC nine-story frame.
 517
 518

Table 5. Damage index for detecting damage at connection B1 in Test 2.

Damage case	Excitation	Damage index (%)					
		S11	S12	S13	S14	S15	S16
Case 3	AmbE	-47.9	-51.6	-35.0	-36.3	-32.3	-35.5
	WN1	-47.8	-51.6	-35.3	-36.3	-34.0	-33.7
	WN2	-48.9	-52.1	-35.9	-37.4	-35.0	-35.4
Case 4	AmbE	-96.5	-94.9	-93.2	-89.6	-90.0	-85.1
	WN1	-96.9	-95.0	-93.7	-90.2	-90.2	-85.1
	WN2	-97.0	-95.0	-93.8	-90.2	-90.3	-84.9

519



520

521

522

Figure 18. Comparison of the damage index in tests and simulations.

523

524

525

Figure 18 compares the damage index at sensor S13 obtained in tests and simulations. The numerical relationship of the damage index and the reduced bending stiffness at a fractured section was extracted from the bending moment responses of the finite element model of the five-

526 story frame, in which beams and columns were modeled with beam elements, and the fracture
 527 damage at removable connections was modeled with a simplified crack model presented by Sinha
 528 *et al.* [26]. The experimental damage index of -35% and -93% for damage L1 and L2 matched
 529 well with the numerical values of -33% and -90% . In addition, the relation between the damage
 530 index DI and the reduction in bending stiffness EI_x numerically extracted from the five-story
 531 frame and that constructed from the SAC nine-story frame matched at some extent.

532

533 *4.6.3. Test 3*

534

535 The stability of the damage index was examined by changing the location of damage in the
 536 testbed frame. As given in Table 6, the mean values of the damage index at three different
 537 connections B2, B6, and B10 were -59% , -55% , and -52% for damage L1 and -91% , -92% ,
 538 and -95% for damage L2. The standard deviations in the damage indices for three excitations
 539 were less than 0.7% for damage L1 and 3.9% for damage L2. The variation was larger for the
 540 severer damage condition. The damage index slightly varied for different damage locations but
 541 the observed variation was at most 7.8% for damage L1 and 3.8% for damage L2. This indicated
 542 the general applicability of the damage evaluation based on the proposed damage index for the
 543 presented level of damage.

544

545

Table 6. Damage index for detecting damage L1 and L2 in Test 3.

Damage category	Damage case	Damage index (%)				
		AmbE	WN1	WN2	Mean	Standard deviation
L1	Case 5	-59.6	-60.4	-59.6	-59.9	0.5
	Case 6	-55.2	-55.8	-55.2	-55.4	0.3
	Case 7	-52.0	-51.4	-52.8	-52.1	0.7
L2	Case 8	-87.1	-93.8	-94.0	-91.6	3.9
	Case 9	-89.5	-93.2	-93.6	-92.1	2.3
	Case 10	-94.3	-96.5	-95.4	-95.4	1.1

546

547 *4.6.3. Test 4*

548

549 Another important influential factor for the damage index is the increases of bending moment
 550 sustained at damage-neighboring connections in the moment redistributions. The existence of
 551 severe damage nearby in particular affects the damage index for detecting small damage. Thus, a
 552 systematic approach to identify the extent of damage at multiple locations is needed. As this issue
 553 will be a focus of further developments of the presented method, in Test 4, preliminary test data
 554 for the multiple damage condition was obtained. In Case 12, damage L1 at the left and right sides
 555 of a beam-column connection was considered. The damage index at the right side (i.e.,
 556 connection B3) increased approximately by 5% with the existence of the left side damage
 557 compared to those for the single damage condition in Case 11 (i.e., from -55.5% to -49.3% in
 558 mean). The damage index further increased by 15% (i.e., from -49.3% to -34.1% in mean) with
 559 the existence of damage L2 in Case 13. In contrast, when damage L2 existed nearby beam-
 560 column connections in Case 14, the increment was only around 5% . In Cases 16 and 17, damage
 561 L2 was considered at two locations. The results indicate that the influence was negligible at this
 562 severity of damage compared to that for the single damage condition in Case 15.

563

564

Table 7. Damage index for detecting damage L1 and L2 at connection B3 in Test 4.

Damage category	Damage case	Damage index (%)				
		AmbE	WN1	WN2	Mean	Standard deviation
L1	Case 11	-55.9	-55.1	-55.5	-55.5	0.4
	Case 12	-49.7	-49.1	-49.1	-49.3	0.3
	Case 13	-34.8	-34.1	-33.5	-34.1	0.7
	Case 14	-50.3	-50.9	-50.4	-50.5	0.3
L2	Case 15	-92.0	-93.2	-93.1	-92.8	0.7
	Case 16	-90.4	-91.6	-91.3	-91.1	0.6
	Case 17	-92.4	-99.1	-99.0	-96.8	3.8

565

566

567

568

5. CONCLUSIONS

569 This paper presented the development of a strain-based damage index for detecting beam fracture
570 damage in steel moment-resisting frames. The effectiveness of the damage index was numerically
571 and experimentally verified using an SAC nine-story steel frame and a five-story steel frame
572 testbed. The notable findings are summarized as follows.

573 (1) The independency of the presented damage index on the characteristics of external
574 excitations and the selection of vibration modes was verified in numerical simulations and
575 shaking table tests. As the extraction of modal responses required preset band-pass filters, the use
576 of dominant vibration modes with clear responses and high power was highly desirable.

577 (2) Both in the numerical simulations and experiments, the damage index extracted within a
578 distance of $1.2d$ (d is beam depth) from a fracture was largely affected by local strain
579 redistributions induced by the fracture. A distance between $1.2d$ and $2.0d$ from the fracture was
580 recommended for evaluating the moment redistributions in steel moment-resisting frames and the
581 reduction in bending stiffness at fractured sections.

582 (3) The relationship between the damage index DI and the reduction in the bending stiffness
583 EI_x of fracture sections was estimated from numerical simulations. The experimental damage
584 indices for damage L1 and L2 in the five-story frame matched very well with the numerical
585 values with the difference of less than 3%. The relationship allows the evaluation of the damage
586 extent at beam-ends from the damage index extracted from measurement data.

587 (4) Consistency of the damage index in the evaluation of damage at different locations was
588 verified in experimental studies using the five-story steel testbed frame. The level of variation
589 was at most 7.8% for damage L1 with fracture of the bottom flange and 3.8% for damage L2 with
590 fracture of the bottom flange and web.

591 (5) The proposed method is a strategy for local damage identification. A detecting sensor is
592 used to detect and quantify a seismic fracture at the beam end. Thus, for evaluating the damage
593 state of an entire building, a dense array of sensors is needed to cover all beam ends that may
594 develop fractures or critical regions. However, the number of sensors allocated can be reduced by
595 pre-identifying damage-prone beams at stories sustaining large drift, which are likely to be the
596 lower stories, or by integrating other information (e.g., maximum story responses measured using
597 accelerometers). Monitoring beams of large-deformation floors would be effective in assessing
598 the safety of the building.

599 (6) Future studies are needed to quantify and systematically filter out the influence of
600 neighboring beam damage on the damage index when there is multiple beam damage, and to

601 evaluate the influence of other damaged structural components (e.g., breakdown of the composite
 602 action in concrete slabs) on the damage index. It is also desirable to generalize the relationship
 603 between the damage index and the damage extent for different configurations of frame
 604 dimensions and beam sizes.

605
 606
 607
 608

ACKNOWLEDGEMENTS

609 The authors gratefully acknowledge funding support offered by the General Collaborative
 610 Research program of the Disaster Prevention Research Institute, Kyoto University under Project
 611 Number 24A-05 (PI: Masahiro Kurata). The greatest of thanks go to Dr. Lin Xuchuan for
 612 numerical simulation work using Marc software and Dr. Tang Zhenyun and Ms. Mayako
 613 Yamaguchi for assistance offered in the experimental work.

614
 615

REFERENCES

616
 617

- 618 1. Nakashima M. Reconnaissance report on damage to steel buildings structures observed from
 619 the 1995 Hyogoken-Nanbu (Hanshin/Awaji) earthquake, Abridged English edition. Steel
 620 Committee of Kinki Branch, the Architectural Institute of Japan (AIJ), 1995.
- 621 2. Mahin S. Lessons from damage to steel buildings during the Northridge earthquake.
 622 *Engineering Structures* 1998; 20(4-6): 261-270. DOI: 10.1016/S0141-0296(97)00032-1.
- 623 3. Fan W, Qiao P. Vibration-based damage identification methods: a review and comparative
 624 study. *Structural health monitoring* 2011; 10(1): 83-111. DOI: 10.1177/1475921710365419.
- 625 4. Celebi M, Sanli A, Sinclair M, Gallant S, Radulescu D. Real-time seismic monitoring needs
 626 of a building owner - and the solution: a cooperative effort. *Earthquake Spectra* 2004; 20(2),
 627 333-346. DOI: 10.1193/1.1735987.
- 628 5. Todorovska MI, Trifunac MD. Impulse response analysis of the Van Nuys 7-storey hotel
 629 during 11 earthquakes and earthquake damage detection. *Structural Control and Health*
 630 *Monitoring* 2008; 15(1): 90-116. DOI: 10.1002/stc.208.
- 631 6. Sohn H, Farrar CR. Damage diagnosis using time series analysis of vibration signals. *Smart*
 632 *Materials and Structures* 2001; 10(3), 446-451. DOI:10.1088/0964-1726/10/3/304.
- 633 7. Naeim F, Hagie H, Alimoradi A, Miranda E. Automated post-earthquake damage assessment
 634 and safety evaluation of instrumented buildings. A Report to CSMIP (JAMA Report No.
 635 2005-10639), John A. Martin & Associates, 2005.
- 636 8. Kalkan E, Banga K, Ulusoy HS, Fletcher JPB, Leith WS, Reza S, Cheng T. Advanced
 637 earthquake monitoring system for U.S. Department of Veterans Affairs medical buildings—
 638 instrumentation. U.S. Geological Survey Open-File Report 2012-1241, 143 p, 2012.
- 639 9. Ji X, Fenves G, Kajiwara K, Nakashima M. Seismic damage detection of a full-scale shaking
 640 table test structure. *Journal of Structural Engineering* 2011; 137(6): 14-21. DOI:
 641 10.1061/(ASCE)ST.1943-541X.0000278.
- 642 10. Chung Y. Existing performance and effect of retrofit of high-rise steel buildings subjected to
 643 long-period ground motions. Doctoral Dissertation, Kyoto University, Japan, 2010.
- 644 11. Li S, Wu Z. Development of distributed long-gage fiber optic sensing system for structural
 645 health monitoring. *Structural health monitoring* 2007; 6(2): 133-143. DOI:
 646 10.1177/1475921706072078.

- 647 12. Hong W, Wu Z, Yang C, Wan C, Wu G. Investigation on the damage identification of
648 bridges using distributed long-gauge dynamic macrostrain response under ambient excitation.
649 *Journal of Intelligent Material Systems and Structures* 2012; 23(1): 85-103. DOI:
650 10.1177/1045389X11430743.
- 651 13. Razi P, Esmaeel RA, Taheri F. Improvement of a vibration-based damage detection approach
652 for health monitoring of bolted flange joints in pipelines. *Structural health monitoring* 2013;
653 12(3): 207-224. DOI: 10.1177/1475921713479641.
- 654 14. Mujica LE, Vehi J, Staszewski W, Worden K. Impact damage detection in aircraft
655 composites using knowledge-based reasoning. *Structural health monitoring* 2008; 7(3): 215-
656 230. DOI: 10.1177/1475921708090560.
- 657 15. Lynch JP, Loh KJ. A summary review of wireless sensors and sensor networks for structural
658 health monitoring. *The Shock and Vibration Digest* 2006; 38(2): 91-128. DOI:
659 10.1177/0583102406061499.
- 660 16. Pakzad SN, Fenves GL. Statistical analysis of vibration modes of a suspension bridge using
661 spatially dense wireless sensor network. *Journal of Structural Engineering* 2009; 135(7):
662 863-872. DOI: 10.1061/(ASCE)ST.1943-541X.0000033.
- 663 17. Kurata M, Kim J, Lynch JP, van der Linden GW, Sedarat H, Thometz E, Hipley P, Sheng LH.
664 Internet-enabled wireless structural monitoring systems: Development and permanent
665 deployment at the New Carquinez suspension bridge. *Journal of Structural Engineering* 2013;
666 139(10): 1688-1702. DOI: 10.1061/(ASCE)ST.1943-541X.0000609.
- 667 18. Park G, Inman DJ. Structural health monitoring using piezoelectric impedance measurements.
668 *Philosophical Transactions of the Royal Society A* 2007; 365: 373-392. DOI:
669 10.1098/rsta.2006.1934.
- 670 19. Kurata M, Li X, Fujita K, Yamaguchi M. Piezoelectric dynamic strain monitoring for
671 detecting local seismic damage in steel buildings. *Smart Materials and Structures* 2013; 22,
672 115002. DOI:10.1088/0964-1726/22/11/115002.
- 673 20. Chopra AK. *Dynamics of structures: theory and applications to earthquake engineering, 2th*
674 *edition*. Prentice Hall, 2001.
- 675 21. FEMA-355C. *State of the art report on systems performance of steel moment frames subject*
676 *to earthquake ground shaking*, 2000.
- 677 22. MSC Software Corporation. <http://www.mscsoftware.com/product/marc> [30 Dec. 2013].
- 678 23. Ohtori Y, Christenson RE, Spencer BF, Dyke SJ. Benchmark control problems for
679 seismically excited nonlinear buildings. *Journal of Engineering Mechanics* 2004; 130(4):
680 366-385. DOI: 10.1061/(ASCE)0733-9399(2004)130:4(366).
- 681 24. Measurement Specialties. <http://www.meas-spec.com> [30 Dec. 2013].
- 682 25. Civionics, LLC. <http://www.civionics.com> [30 Dec. 2013].
- 683 26. Sinha JK, Friswell MI, Edwards S. Simplified models for the location of cracks in beam
684 structures using measured vibration data. *Journal of Sound and Vibration* 2002; 251(1):13-38.
685 DOI: 10.1006/jsvi.2001.3978.